Colloid Polym Sci (2005) 283: 627–635
DOI 10.1007/s00396-004-1193-1

ORIGINAL CONTRIBUTION

Huan J. Keh
Yu C. Chang

Creeping motion of an assemblage of composite spheres relative to a fluid

Received: 2 April 2004
Accepted: 6 July 2004
Published online: 20 August 2004

H. J. Keh (✉) · Y. C. Chang
Department of Chemical Engineering,
National Taiwan University,
106-17 Taipei, Taiwan
E-mail: huan@ntu.edu.tw
Fax: +886-2-23623040

Abstract The sedimentation of a homogeneous distribution of spherical composite particles and the fluid flow through a bed of these particles are investigated theoretically. Each composite particle is composed of a spherical solid core and a surrounding porous shell. In the fluid-permeable porous shell, idealized hydrodynamic frictional segments are assumed to distribute uniformly. The effect of interactions among the particles is taken into explicit account by employing a fundamental cell-model representation which is known to provide good predictions for the motion of a swarm of non-porous spheres within a fluid. In the limit of a small Reynolds number, the Stokes and Brinkman equations are solved for the flow field in a unit cell, and the drag force exerted by the fluid on the particle is obtained in a closed form. For a distribution of composite spheres, the normalized mobility of the particles decreases or the particle interactions increase monotonically with a decrease in the permeability of their porous shells. The effect of particle interactions on the creeping motion of composite spheres relative to a fluid can be quite significant in some situations. In the limiting cases, the analytical solutions describing the drag force or mobility for a suspension of composite spheres reduce to those for suspensions of solid spheres and of porous spheres. The hydrodynamic behavior for composite spheres may be approximated by that for permeable spheres when the porous layer is sufficiently thick, depending on the permeability.

Keywords Composite sphere · Porous sphere · Creeping flow · Particle interactions · Unit cell model

Introduction

The motion of colloidal particles in a continuous medium at low Reynolds numbers has long been an important subject in the fields of chemical, biomedical, and environmental engineering and science. The majority of these transport phenomena are fundamental in nature, but permit one to develop a rational understanding of many practical systems and industrial processes such as sedimentation, flotation, electrophoresis, agglomeration, and motion of blood cells in an artery or vein. The theoretical study of this subject has grown out of the classic work of Stokes [1] for the creeping motion of a rigid sphere in an unbounded viscous fluid.

The surface of a colloidal particle is generally not hard and smooth as assumed in many theoretical models. For instance, surface layers are purposely formed by adsorbing long-chain polymers to make the suspended particles stable against flocculation [2]. Even the surfaces of model colloids such as silica and polystyrene latex are ''hairy'' with a gel-like polymeric layer extending a

substantial distance into the suspending medium from the bulk material inside the particle [3]. In particular, the surface of a biological cell is not a hard smooth wall, but rather is a permeable rough surface with various appendages ranging from protein molecules on the order of nanometers to cilia on the order of micrometers [4]. Such particles can be modeled as a composite particle having a central solid core and an outer porous shell [5]. When the solid core vanishes, the particle reduces to a permeable one, such as polymer coils [6] or colloidal flocs [7].

The motion of an isolated colloidal sphere covered by a thin layer of adsorbed polymers in an incompressible Newtonian fluid was analyzed by Anderson and Kim [8] using a method of matched asymptotic expansions to solve the Brinkman equation for the flow field within the surface polymer layer and the Stokes equations for the flow field external to the particle. The result for the drag force exerted by the fluid on the moving particle, expressed as the hydrodynamic thickness of the polymer layer, is accurate to $O(\lambda^2)$, where λ is the ratio of the polymer-layer characteristic length to the particle radius. On the other hand, the creeping flow of an incompressible Newtonian fluid past a spherical composite particle with an arbitrary thickness of its permeable shell was solved by Masliyah et al. [9] and Veerapaneni and Wiesner [10] using the Brinkman and Stokes equations. An analytical formula for the drag force experienced by the particle was derived as a function of the radius of the solid core, the thickness of the porous shell, and the permeability of the shell. Masliyah et al. [9] also measured the settling velocity of a solid sphere with attached threads and found that theoretical predictions for the composite sphere are in excellent agreement with the experimental results.

In most practical applications of particle motion relative to a fluid, collections of particles are encountered. Thus, it is important to determine if the presence of neighboring particles significantly affects the movement of an individual particle. Using a method of reflections, Anderson and Solomentsev [3] analytically solved the mobility problem of two arbitrarily oriented, identical composite spheres with thin adsorbed polymer layers. The mobility coefficients accurate to $O(\lambda^2)$ were determined in a power series of h^{-1} up to $O(h^{-5})$, where h is the center-to-center distance between the particles divided by their radius. For the creeping motion of two composite spheres with thin porous layers along the line of their centers, their hydrodynamic interactions were studied through the use of a lubrication theory for the case of particles in near contact [11, 12] and a boundary collocation method for the case of an arbitrary separation distance between the particles [13]. The hydrodynamic interactions among a string of multiple composite spheres with an arbitrary thickness for each of the permeable shells undergoing axisymmetric motion were also examined by using the boundary collocation method [12]. On the basis of a microscopic model of two-particle interactions which involves the concept of statistical mechanics [14, 15], the mobility coefficients of the composite spheres can be used to evaluate approximately the mean settling velocity in a dilute suspension of composite spheres as a function of the particle concentration.

Another technique which has been employed successfully to predict the effect of particle concentration on the particle sedimentation rate is the unit cell model [16, 17, 18]. This model involves the concept that an assemblage can be divided into a number of identical cells, one sphere occupying each cell. The boundary-value problem for multiple spheres is thus reduced to the consideration of the behavior of a single sphere and its bounding envelope. Although different shapes of cells can be employed, the assumption of a spherical shape for the fictitious envelope of fluid surrounding each spherical particle is of great convenience. The cell model is of great applicability in concentrated assemblages, where the effect of container walls will not be important. Prasad et al. [19] analyzed the problem of the creeping flow of a fluid relative to an assemblage of identical composite spheres to some extent using the Happel cell model [16], but their results are incomplete and contain significant errors. In this work, the unit cell model is used to study the hydrodynamic interactions among a swarm of composite spheres with an arbitrary thickness of the porous layers moving relative to a fluid. In addition to the Happel model, the Kuwabara cell model [17] is also considered. The solutions obtained with these models enable the sedimentation rate in a suspension of composite spheres or alternatively the pressure drop for a fluid flow through a bed of composite spheres to be predicted as a function of the microstructure and volume fraction of the particles.

Analysis

We consider the steady body-force-driven motion (e.g., sedimentation) of a uniform three-dimensional distribution of identical spherical composite particles of radius b in an incompressible Newtonian fluid of viscosity η. Each composite sphere has a surface layer of homogeneous porous material of constant thickness $b-a$ and permeability k so that the radius of the rigid impermeable core is a. The average particle velocity equals U in the positive z-direction. As shown in Fig. 1, we employ a unit cell model in which each particle is surrounded by a concentric shell of suspending fluid having an outer radius c such that the particle-to-cell

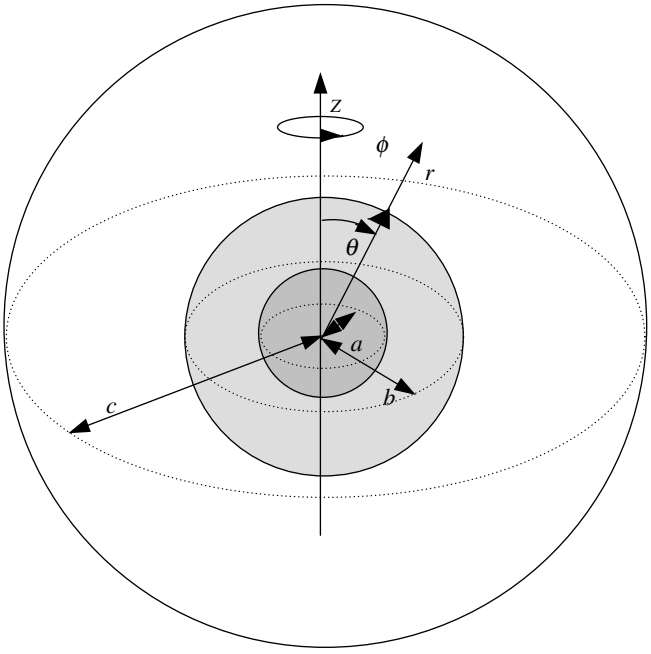

Fig. 1 Geometrical sketch for the relative motion of a spherical composite particle at the center of a spherical cell

volume ratio is equal to the particle volume fraction ϕ throughout the entire suspension; viz., $\phi = (b/c)^3$. The origin of the spherical coordinate system (r,θ,ϕ) is set at the particle center. The Reynolds number is assumed to be sufficiently small so that the inertial terms in the fluid momentum equation can be neglected, in comparison with the viscous terms. Our objective is to determine the hydrodynamic drag force exerted on the particle moving with velocity U in a cell.

The fluid flow external to the composite sphere in a cell ($b \le r \le c$) is governed by the Stokes equations,

$$\eta \nabla^2 \mathbf{v} - \nabla p = \mathbf{0} \tag{1a}$$

and

$$\nabla \cdot \mathbf{v} = 0, \tag{1b}$$

where $\mathbf{v}$ is the fluid velocity field for the flow outside and relative to the particle and p is the corresponding dynamic pressure distribution. For the fluid flow within the porous layer of the particle ($a \le r \le b$), the relative velocity $\mathbf{v}^*$ and dynamic pressure p^* are governed by the Brinkman equation, which is preferred to the Darcy equation to accommodate the boundary conditions at the particle surface ($r = b$),

$$\eta \nabla^2 \mathbf{v}^* - \frac{\eta}{k}\mathbf{v}^* - \nabla p^* = \mathbf{0} \tag{2a}$$

and

$$\nabla \cdot \mathbf{v}^* = 0, \tag{2b}$$

where the asterisk superscript represents a macroscopically averaged quantity pertaining to the porous layer region. Here, we have assumed that the fluid has the same viscosity inside and outside the permeable layer, which is reasonable according to available evidence [8, 20].

Since the flow field in the cell is axially symmetric, it is convenient to introduce the Stokes stream function $\Psi(r,\theta)$ which satisfies Eq. (1b) and is related to the velocity components in the spherical coordinate system by

$$v_r = -\frac{1}{r^2 \sin\theta}\frac{\partial \Psi}{\partial \theta} \tag{3a}$$

and

$$v_\theta = \frac{1}{r \sin\theta}\frac{\partial \Psi}{\partial r}. \tag{3b}$$

Taking the curl of Eq. (1a) and applying Eqs. (3a) and (3b), we obtain a fourth-order linear partial differential equation for Ψ,

$$E_s^4 \Psi = E_s^2 \left(E_s^2 \Psi\right) = 0 \quad \text{if } b \leqslant r \leqslant c, \tag{4}$$

where the axisymmetric Stokes operator E_s^2 is given by

$$E_s^2 = \frac{\partial^2}{\partial r^2} + \frac{\sin\theta}{r^2}\frac{\partial}{\partial \theta}\left(\frac{1}{\sin\theta}\frac{\partial}{\partial \theta}\right). \tag{5}$$

Accordingly, Eqs. (2a) and (2b) can be expressed in terms of the stream function $\Psi^*(r,\theta)$, which is related to the velocity components v_r^* and v_θ^* by Eqs. (3a) and (3b), as

$$E_s^4 \Psi^* - \frac{1}{k} E_s^2 \Psi^* = 0 \quad \text{if } a \leqslant r \leqslant b. \tag{6}$$

Owing to the continuity of velocity and stress components at the outer surface of the porous shell, which is physically realistic and mathematically consistent for the present problem [20, 21], and the no-slip requirement at the solid core surface, the boundary conditions for the flow field at the surfaces of the porous layer are

$r = a$:

$$v_r^* = v_\theta^* = 0 \tag{7}$$

and

$r = b$:

$$v_r^* = v_r, \tag{8a}$$

$$v_\theta^* = v_\theta, \tag{8b}$$

$$\tau_{rr}^* = \tau_{rr}, \tag{9a}$$

$$\tau_{r\theta}^* = \tau_{r\theta}. \tag{9b}$$

Here, τ_{rr} and $\tau_{r\theta}$ are the relevant normal and shear stresses for the fluid flow. Since we take the same fluid viscosity inside and outside the porous shell and use the fluid velocity continuity given by Eqs. (8a) and (8b), Eq. (9a) is equivalent to the continuity of pressure ($p^* = p$ at $r = b$).

On the outer (virtual) boundary of the cell, the Happel model assumes that the radial velocity and the shear stress of the fluid are zero [16]; viz.,

$r = c$:

$$v_r = -U\cos\theta, \tag{10a}$$

$$\tau_{r\theta} = 0. \tag{10b}$$

Equations (7), (8a), (8b), (9a), (9b), (10a), and (10b) take a reference frame that the composite sphere is at rest and the radial velocity of the fluid at the outer boundary of the cell is that of the particle in the opposite direction.

A solution to Eqs. (4) and (6) suitable for satisfying boundary conditions on the spherical surfaces is

$$\Psi = \frac{1}{2}kU\left(A\xi^{-1} + B\xi + C\xi^2 + D\xi^4\right)\sin^2\theta \quad \text{if } \beta \leqslant \xi \leqslant \gamma, \tag{11a}$$

$$\Psi^* = \frac{1}{2}kU\left[E\xi^{-1} + F\xi^2 + G\left(\xi^{-1}\cosh\xi - \sinh\xi\right) + H\left(\xi^{-1}\sinh\xi - \cosh\xi\right)\right]\sin^2\theta \quad \text{if } \alpha \leqslant \xi \leqslant \beta, \tag{11b}$$

where the dimensionless variables $\xi = r/k^{1/2}$, $\alpha = a/k^{1/2}$, $\beta = b/k^{1/2}$, and $\gamma = c/k^{1/2}$. The dimensionless constants A, B, C, D, E, F, G, and H are found from Eqs. (7), (8a), (8b), (9a), (9b), (10a), and (10b) using Eqs. (3a) and (3b). The procedure is straightforward but tedious, and the result is given in the Appendix.

The drag force (in the z-direction) exerted by the external fluid on the composite sphere with the spherical boundary $r = b$ can be determined from [9, 18]

$$F_{\mathrm{d}} = 4\pi\eta k^{1/2} UB, \tag{12}$$

where B is given by Eq. (33). In the limiting case of $\beta/\gamma = b/c = 0$, Eq. (12) becomes

$$F_{\mathrm{d}}^{(0)} = -6\pi\eta k^{1/2} Uf, \tag{13}$$

where

$$f = \left[\beta\lambda - 3\alpha^2 - \left(\lambda - 3\alpha^2\beta\right)\tanh(\beta - \alpha)\right] \times \left[\lambda + 3\beta + 3\left(\alpha^2 - 1\right)\tanh(\beta - \alpha) - 6\alpha\,\mathrm{sech}(\beta - \alpha)\right]^{-1}, \tag{14a}$$

and

$$\lambda = 2\beta^3 + \alpha^3 + 3\alpha. \tag{14b}$$

The formula given by Eq. (13) is the reduced result for the motion of an isolated composite sphere in the absence of the other ones obtained by Masliyah et al. [9].

Through the use of Eqs. (12) and (13), the normalized mobility of the composite sphere in a unit cell can be expressed as

$$M = \frac{F_{\mathrm{d}}^{(0)}}{F_{\mathrm{d}}} = -\frac{3f}{2B}. \tag{15}$$

Note that $M = 1$ as $\beta/\gamma = \phi^{1/3} = 0$ and $0 \leq M < 1$ as $0 < \beta/\gamma \leq 1$. The presence of the virtual surface of the cell always enhances the hydrodynamic drag on the particle since the radial fluid flow vanishes there as required by Eq. (10a).

When $\beta = \alpha$ or $k \to \infty$, $F_{\mathrm{d}}^{(0)} = -6\pi\eta aU$ (Stokes' law) and Eq. (15) reduces to

$$M = \left(1 - \frac{3}{2}\varphi^{1/3} + \frac{3}{2}\varphi^{5/3} - \varphi^2\right)\left(1 + \frac{2}{3}\varphi^{5/3}\right)^{-1}, \tag{16}$$

where $\phi = (a/c)^3$. This is the result for the motion of a rigid sphere of radius a in a cell of radius c.

When $\alpha = \beta$ or $k = 0$, $F_{\mathrm{d}}^{(0)} = -6\pi\eta bU$ and Eq. (15) still reduces to Eq. (16) with $\phi = (b/c)^3$. This result corresponds to the motion of a rigid sphere of radius b in a cell of radius c.

When $a = 0$, Eqs. (13) and (15) become

$$F_{\mathrm{d}}^{(0)} = -6\pi\eta bU\frac{2\beta^2(\beta - \tanh\beta)}{2\beta^2 + 3(\beta - \tanh\beta)} \tag{17}$$

and

$$M = 3\left(\beta - \tanh\beta\right)\left\{\beta\left[3s_1 + \beta^2 s_3 - 30\beta^5 - \beta^2\left(s_2 - 60\beta^3\right)\varphi^{1/3}\right] - 3\left[s_4 + 5\beta^7 + 10\beta^5 - \beta^2\left(s_1 - 20\beta^3\right)\varphi^{1/3}\right]\tanh\beta\right\} \times \left[\beta\left(2\beta^2 + 3\right) - 3\tanh\beta\right]^{-1} \times \left[\beta\left(s_2 - 60\beta^3\right) - 3\left(s_1 - 20\beta^3\right)\tanh\beta\right]^{-1}, \tag{18}$$

where the dimensionless parameters s_1, s_2, s_3, and s_4 are defined by Eq. (41) in the Appendix. The hydrodynamic drag and normalized mobility given by Eqs. (17) and (18) describe the motion of a porous (permeable) sphere of radius b in an unbounded fluid [21] and in a cell of radius c, respectively.

The unit cell model can also be applied to the case of a fluid flow through a bed of composite spheres. For the model under consideration, the drag force F_{d} divided by the cell volume $(4/3)\pi c^3$ will equal $-\Delta P/L$, the pressure drop per unit length of bed due to passage of fluid

through it. Use of this relationship and Eq. (12) gives the superficial fluid velocity through the bed as

$$U = \left(-\frac{\beta b^2}{3B\varphi}\right)\frac{\Delta P}{\eta L}, \tag{19}$$

where the quantity in parentheses is the permeability coefficient in the Darcy law for the whole bed. If we use $U^{(0)}$ and $\Delta P^{(0)}$ to represent U and ΔP, respectively, in the limit of $\phi \to 0$ (a loose bed), the ratio $U/U^{(0)}$ with $\Delta P = \Delta P^{(0)}$ (equals the ratio $\Delta P^{(0)}/\Delta P$ with $U = U^{(0)}$) is also equal to the normalized mobility M given by Eq. (15).

If the Kuwabara model for the boundary condition of the fluid flow at the virtual surface of the cell, which assumes that the radial velocity and the vorticity are zero [17], is used, Eq. (10b) is replaced by

$$r = c: \quad (\nabla \times \mathbf{v})_\phi = \frac{\partial v_\theta}{\partial r} + \frac{v_\theta}{r} - \frac{1}{r}\frac{\partial v_r}{\partial \theta} = 0. \tag{20}$$

With this change, the stream functions Ψ and Ψ^* and the drag force F_d can still be expressed in the forms of Eqs. (11a), (11b), and (12), but the coefficients A, B, C, D, E, F, G, and H should be determined by the boundary conditions in Eqs. (7), (8a), (8b), (9a), (9b), (10a), and (20). The result is given in the Appendix (B is given by Eq. 44). It is easy to find that, for the case of the Kuwabara model, Eqs. (16) and (18) for the normalized particle mobility become

$$M = 1 - \frac{9}{5}\varphi^{1/3} + \varphi - \frac{1}{5}\varphi^2 \tag{21}$$

and

$$\begin{aligned} M = \frac{1}{5\beta^3}\Big\{\beta\Big[\beta^2\left(2t_7 + 60\beta\right)\varphi^2 + 15t_4\varphi + 2\beta^4 t_1\varphi^{1/3}\Big] \\ - \Big[6\beta^2\left(t_6 + 25\beta\right)\varphi^2 \\ + 15t_4\varphi - 18\beta^5\varphi^{1/3}\Big]\tanh\beta\Big\} \\ \times \Big[\beta\left(2\beta^2 + 3\right) - 3\tanh\beta\Big]^{-1}, \end{aligned} \tag{22}$$

respectively. In Eq. (22), the dimensionless parameters t_1, t_4, t_6, and t_7 are given by Eq. (52). It can be seen in Eqs. (16) and (21) that the leading order of the particle concentration effect on the particle mobility is $\phi^{1/3}$ and this effect predicted by the Kuwabara model is stronger than that for the Happel model.

Results and discussion

The variation of the normalized mobility M for the motion of a homogeneous distribution of porous spheres (with $a = 0$ or $\alpha/\beta = 0$) given by Eqs. (18) and (22) for the Happel and Kuwabara models, respectively, with the volume fraction ϕ of the particles for various values of β from zero to infinity is displayed in Fig. 2. The calculations are presented up to $\phi = 0.74$, which corresponds to the maximum attainable volume fraction for a swarm of identical spheres [22]. It is also clear that at volume fractions approaching this, agglomeration due to contacts between particles may occur, and the present study does not cover the case. The curve with $\beta = 0$ (or $k \to \infty$) represents the result for porous spheres with no resistance to the fluid flow, while the curve with $\beta \to \infty$ (or $k = 0$) denotes the result for solid particles. As expected, the normalized mobility M equals unity as $\beta = 0$ for any value of ϕ and is a monotonic decreasing function of ϕ for any given value of $\beta > 0$. Obviously, the particle interaction effect on the mobility (or drag force) is stronger when the permeability k of the particles is smaller (or β is greater). For $\beta < 1$, the particle mobility varies slowly with the volume fraction ϕ, compared with the case of a lower permeability (or greater β). This weak dependence can be explained by the fact that, instead of bypassing, the fluid can easily flow through the porous particle with a high permeability, thereby reducing the hydrodynamic interaction among particles. For $\beta > 10$, the value of the particle mobility is quite close to that of solid particles (with $\beta \to \infty$) when ϕ is small, but the difference becomes more significant as the particles get closer to one another. This implies that, far from the others, a porous particle with a low permeability behaves like a solid one with most fluid flowing over it.

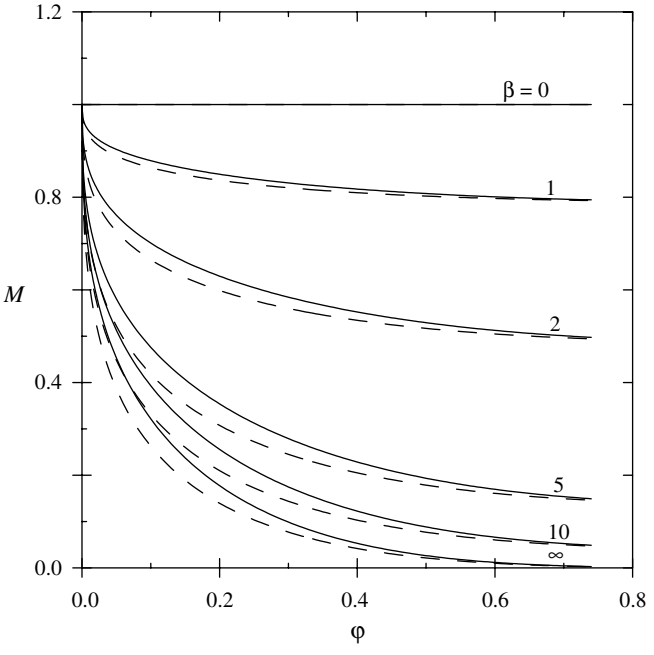

Fig. 2 Normalized particle mobility M in a suspension of identical porous spheres ($a = 0$) versus the particle volume fraction ϕ for various values of β

When the neighboring porous particles become sufficiently close together, a large pressure gradient is developed in-between to drive more fluid to permeate through the porous medium [12]. Interestingly, for cases with a finite value of β, the particle mobility does not vanish even as the particle touches its neighbors. For constant values of β and ϕ, the Kuwabara model predicts a stronger concentration effect on the particle mobility (or a smaller mean particle mobility) than the Happel model does. This occurs because the zero-vorticity model yields a larger energy dissipation in the cell than that due to particle drag alone, owing to the additional work done by the stresses at the outer boundary [18]. In general cases, the predictions of the two models are in numerical agreement to within 15% and result in the same behavior qualitatively.

On the basis of the numerical solution of the hydrodynamic interactions between pairs of settling porous spheres obtained by the boundary collocation method, Chen and Cai [23] also derived an ensemble-averaged formula for the mean particle mobility in a dilute suspension of identical porous spheres (say, $\phi < 0.1$) in the form

$$M = 1 - \alpha_1 \varphi + O(\varphi^2). \tag{23}$$

They found that the value of α_1 (which is always positive) increases with an increase in β. As examples, $\alpha_1 = 5.50$ as $\beta = 10$ and $\alpha_1 = 6.44$ as $\beta = 100$. Note that M varies linearly with ϕ in Eq. (23), while Eqs. (16), (18), (21), and (22) indicate that M depends linearly on $\phi^{1/3}$ for the cell model when the value of ϕ is small.

After understanding the particle interaction effect on the motion of porous spheres, we now examine the general case of the motion of a swarm of composite spheres. The normalized mobility M is shown in Fig. 3a and b as a function of the volume fraction ϕ and the parameter α/β over the entire possible range for the cases of $\beta = 5$ and 1, respectively. Again, M decreases monotonically with an increase in ϕ for fixed values of α/β and β and with an increase in β for constant values of α/β and ϕ. The curve with $\alpha/\beta = 1$ represents the result for a rigid sphere (given by Eqs. 16, 21) and the curve with $\alpha/\beta = 0$ denotes that for a porous sphere (given by Eqs. 18, 22). All the other curves for composite spheres lie between these lower and upper bounds and M is a monotonic decreasing function of α/β for given values of β and ϕ. Namely, the hydrodynamic drag acting on a particle is reduced as its porous layer becomes thick for a given particle size, permeability, and separation distance to its neighbors. It can be seen that, for the case of $\beta = 5$, the behavior of composite spheres with $\alpha/\beta = 0.6$ can be roughly approximated by that of porous ones of equal size and permeability when $\phi < 0.2$. This is because when a porous layer has a low to moderate permeability, it is difficult for the fluid to penetrate deep to reach the core

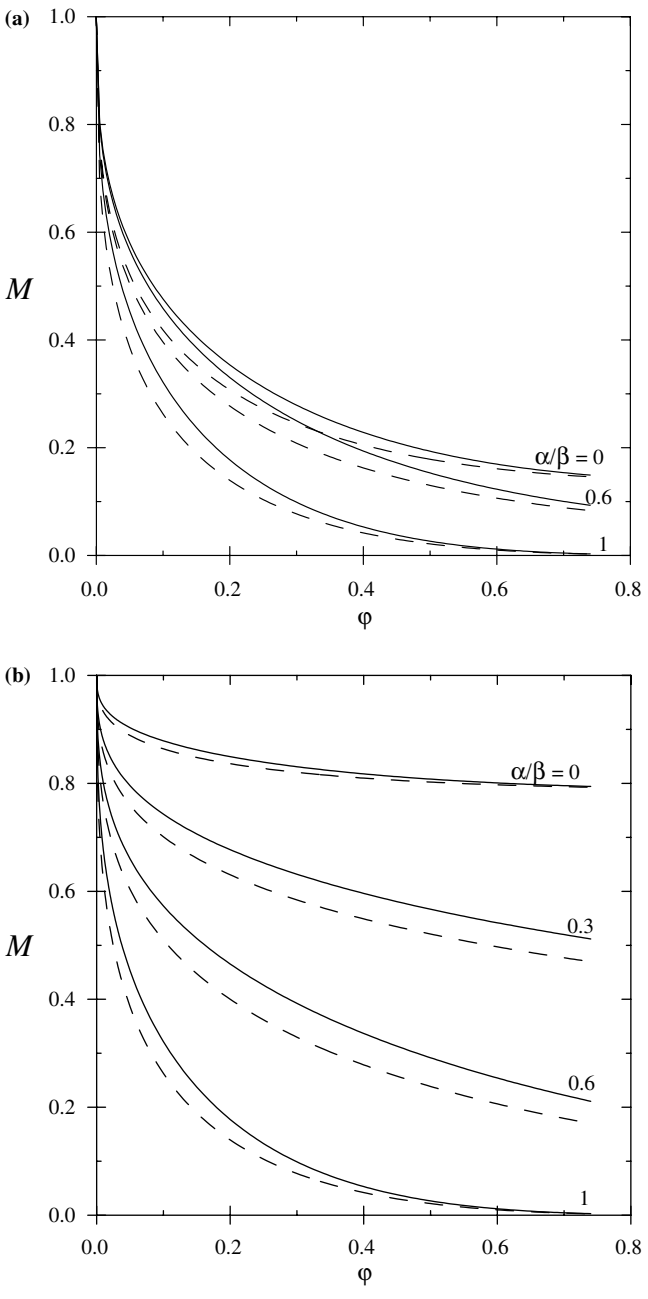

Fig. 3 Normalized particle mobility M in a suspension of identical composite spheres versus the particle volume fraction ϕ for various values of α/β: **a** $\beta = 5$; **b** $\beta = 1$

surface as long as the layer is sufficiently thick and the neighboring particles are not too close. Thus, the solid core hardly feels a relative fluid motion, merely exerting a negligibly small resistant force on the fluid [9, 12]. However, this approximation is no longer valid for a porous layer with a large permeability, as for the case of $\beta = 1$ shown in Fig. 3b. Again, for cases with $\alpha/\beta < 1$, the particle mobility is not necessarily equal to zero as the neighboring particles touch one another.

Concluding remarks

The creeping motion of a swarm of identical composite spheres (which can reduce to solid spheres and porous spheres in the limiting cases) relative to an incompressible Newtonian fluid has been analyzed using the Happel and Kuwabara cell models in this work. In a cell, the Stokes and Brinkman equations for the fluid flow field were solved and the hydrodynamic drag force exerted on the particle as a function of the parameters α/β ($=a/b$), ϕ [$=(b/c)^3$], and β was obtained in closed-form expressions. It was found that the strength of the hydrodynamic interaction between composite spheres falls between the corresponding value for solid spheres and that for porous spheres with the same permeability. For a suspension of particles with fixed values of α/β and ϕ, the mobility of each particle normalized by its corresponding value in the absence of the other ones is a monotonic decreasing function of the parameter β (or an increasing function of the permeability k of the porous surface layer) of the particle. For given values of α/β and β, this normalized mobility decreases monotonically with an increase in the particle volume fraction ϕ. The particle mobility may not vanish even when the neighboring particles touch one another. The analysis assumes that the porous shell of each composite sphere is nondeformable. The result would be very different, particularly in the case where the value of ϕ is large, if the porous shell were able to deform in response to the flow (as might be expected for a layer composed of entangled polymer).

Our results, which provide useful insights into the actual phenomena regarding the creeping motion of composite/porous particles in a suspension, show that the effect of hydrodynamic interactions on the particle motion can be significant in some situations. Both the Happel and Kuwabara models give essentially the same fluid velocity field and approximately equal particle mobility for the motion of composite spheres. However, the Happel model has a significant advantage in that it does not require an exchange of mechanical energy between the cell and the environment [18]. The relevant experimental data, which are not available in the literature, would be needed to confirm the validity of the cell model at various ranges of α/β, β, and ϕ.

Acknowledgement This research was supported by the National Science Council of the Republic of China.

Appendix

For conciseness algebraic equations for the determination of the coefficients in Eqs. (11a) and (11b) as well as their solutions are presented in this appendix.

Applying the boundary conditions given by Eqs. (7), (8a), (8b), (9a), (9b), (10a), and (10b) for the Happel model to the general solution given by Eqs. (11a) and (11b) for the motion of a composite sphere in a concentric spherical cell, one obtains

$$E + F\alpha^3 + G(\cosh\alpha - \alpha\sinh\alpha) + H(\sinh\alpha - \alpha\cosh\alpha) = 0, \tag{24}$$

$$E - 2F\alpha^3 + G\left[\left(\alpha^2+1\right)\cosh\alpha - \alpha\sinh\alpha\right] + H\left[\left(\alpha^2+1\right)\sinh\alpha - \alpha\cosh\alpha\right] = 0, \tag{25}$$

$$A + B\beta^2 + C\beta^3 + D\beta^5 = E + F\beta^3 + G(\cosh\beta - \beta\sinh\beta) + H(\sinh\beta - \beta\cosh\beta), \tag{26}$$

$$A - B\beta^2 - 2C\beta^3 - 4D\beta^5 = E - 2F\beta^3 + G\left[\left(\beta^2+1\right)\cosh\beta - \beta\sinh\beta\right] + H\left[\left(\beta^2+1\right)\sinh\beta - \beta\cosh\beta\right], \tag{27}$$

$$6A + 6D\beta^5 = 6E + 3\left(\beta^2+2\right)(G\cosh\beta + H\sinh\beta) - \beta\left(\beta^2+6\right)(G\sinh\beta + H\cosh\beta), \tag{28}$$

$$2B + 20D\beta^3 = E - 2F\beta^3, \tag{29}$$

$$A + B\gamma^2 + C\gamma^3 + D\gamma^5 = \gamma^3, \tag{30}$$

and

$$A + D\gamma^5 = 0. \tag{31}$$

These simultaneous algebraic equations can be solved to yield the eight unknown constants as

$$A = -\gamma^5 D, \tag{32}$$

$$B = \Delta[-120\alpha\beta^6 - \left(120\beta^7 + 9\alpha^2 s_1 - \beta\lambda s_2\right)\cosh(\beta-\alpha) + 3\left(40\beta^6 - \lambda s_1 + \alpha^2\beta s_2\right)\sinh(\beta-\alpha)], \tag{33}$$

$$C = \Delta\Big\{12\alpha\left(s_4 - 5\beta^5\right) + \left(120\beta^6 + 45\alpha^2\beta^4 - \lambda s_3 - 6\beta s_4\right)\cosh\left(\beta-\alpha\right) + 3\Big[5\beta^4\lambda + 2\left(s_4 + 10\beta^5\right) - \alpha^2 s_3\Big]\sinh\left(\beta-\alpha\right)\Big\}, \tag{34}$$

$$D = \Delta\beta^2\left\{-6\alpha\beta + \left(12\beta^2 + \beta\lambda - 9\alpha^2\right)\cosh\left(\beta-\alpha\right) - 3\left[\lambda - \beta\left(\alpha^2 - 4\right)\right]\sinh\left(\beta-\alpha\right)\right\}, \tag{35}$$

$$E = 6\Delta\alpha\Big[2\beta^3\left(s_5 - 30\beta^3\right) + \left(\beta s_0 s_1 - 3\alpha s_4\right)\cosh(\beta-\alpha) + \left(3\alpha\beta s_1 - s_0 s_4\right)\sinh(\beta-\alpha)\Big], \tag{36}$$

$$F = 6\Delta[\alpha s_5 - \beta s_1\cosh\left(\beta-\alpha\right) + s_4\sinh\left(\beta-\alpha\right)], \tag{37}$$

$$G = 6\Delta\Big[3\alpha^2 s_5\cosh\alpha - 3\alpha\beta s_1\cosh\beta - \big(\lambda s_5 - 60\beta^6\big)\sinh\alpha + 3\alpha s_4\sinh\beta\Big], \tag{38}$$

and

$$H = 6\Delta\Big[\big(\lambda s_5 - 60\beta^6\big)\cosh\alpha - 3\alpha\big(s_4\cosh\beta\alpha s_5\sinh\alpha - \beta s_1\sinh\beta\big)\Big], \tag{39}$$

where

$$\Delta = \gamma\{\big[\gamma\big(60\beta^6 + 45\alpha^2\beta^4 - 6\beta s_1 - \lambda s_3\big) - 120\beta^7 - 9\alpha^2 s_1 + \beta\lambda s_2\big]\cosh\big(\beta-\alpha\big) + 3\big[\gamma\big(20\beta^5 + 5\beta^4\lambda + 2s_4 - \alpha^2 s_3\big) + 40\beta^6 + \alpha^2\beta s_2 - \lambda s_1\big]\sinh\big(\beta-\alpha\big) + 12\alpha\big[\gamma\big(s_4 - 5\beta^5\big) - 10\beta^6\big]\}^{-1}, \tag{40}$$

and

$$s_0 = \alpha^2 + 3, \qquad s_1 = \gamma^5 + 4\beta^5 + 30\beta^3, \qquad s_2 = 3\gamma^5 + 2\beta^5 + 90\beta^3,$$
$$s_3 = 2\gamma^5 + 3\beta^5 + 60\beta^3, \quad s_4 = \gamma^5 + 14\beta^5 + 30\beta^3, \quad s_5 = \gamma^5 - \beta^5 + 30\beta^3. \tag{41}$$

When the Kuwabara model is used, one can apply the boundary conditions given by Eqs. (7), (8a), (8b), (9a), (9b), (10a), and (20) to the general solution given by Eqs. (11a) and (11b) to yield Eqs. (24), (25), (26), (27), (28), (29), (30), and1

$$B - 5D\gamma^3 = 0. \tag{42}$$

Simultaneous solution of these eight algebraic equations leads to

$$A = \frac{1}{2}\Delta'\beta^2\big\{30\alpha\beta\big(t_4 - 8\beta^3\big) - \big[60\beta^2\gamma^3 + \beta\lambda t_6 - 60\alpha\beta^2 s_0 - 9\alpha^2\big(t_6 - 2\beta^3\big)\big]\cosh\big(\beta-\alpha\big) + 3\big[\lambda\big(t_6 - 2\beta^3\big) - \alpha^2\beta\big(t_6 - 60\beta\big) + 20\beta t_3\big]\sinh\big(\beta-\alpha\big)\big\}, \tag{43}$$

$$B = 5\gamma^3 D, \tag{44}$$

$$C = \frac{5}{2}\Delta'\big[6\alpha t_5 + \big(9\alpha^2\beta^2 - \lambda t_5 - 6\beta t_3\big)\cosh\big(\beta-\alpha\big) + 3\big(\beta^2\lambda + 2t_3 - \alpha^2 t_5\big)\sinh\big(\beta-\alpha\big)\big], \tag{45}$$

$$D = \frac{3}{2}\Delta'\big[\big(\beta\lambda - 3\alpha^2\big)\cosh\big(\beta-\alpha\big) - \big(\lambda - 3\alpha^2\beta\big)\sinh\big(\beta-\alpha\big)\big], \tag{46}$$

$$E = 15\Delta'\alpha\big[2\beta^3 t_2 + (\beta s_0 - 3\alpha)t_3\cosh(\beta-\alpha) + (3\alpha\beta - s_0)t_3\sinh(\beta-\alpha)\big], \tag{47}$$

$$F = 15\Delta'\big[\alpha t_2 - \beta t_3\cosh\big(\beta-\alpha\big) + t_3\sinh\big(\beta-\alpha\big)\big], \tag{48}$$

$$G = 15\Delta'\big(3\alpha^2 t_2\cosh\alpha - 3\alpha\beta t_3\cosh\beta - \lambda t_2\sinh\alpha + 3\alpha t_3\sinh\beta\big), \tag{49}$$

and

$$H = 15\Delta'\Big[\lambda t_2\cosh\alpha - 3\alpha(t_3\cosh\beta + \alpha t_2\sinh\alpha - \beta t_3\sinh\beta)\Big], \tag{50}$$

where

$$\Delta' = \gamma^3\big\{\big[9\alpha^2\beta^2\big(t_6 + 15\beta\big) - \big(\beta^3 t_7 + \gamma^5 t_1\big)\lambda - 60\beta^7 - 15\beta\gamma^3 t_4 - 27\alpha^2\gamma^5\big]\cosh\big(\beta-\alpha\big) + 3\big[\beta^2\lambda\big(t_6 + 15\beta\big) - 3\gamma^5\lambda + 20\beta^6 + 5\gamma^3 t_4 - \alpha^2\big(\beta^3 t_7 + \gamma^5 t_1\big)\big]\sinh\big(\beta-\alpha\big) + 30\alpha t_2 t_3\big\}^{-1}, \tag{51}$$

and

$$t_1 = 5\gamma - 9\beta, \qquad t_2 = \gamma^3 - \beta^3, \quad t_3 = \gamma^3 + 2\beta^3,$$
$$t_4 = \gamma^3 + 4\beta^3, \qquad t_5 = 2\gamma^3 + \beta^3, \quad t_6 = 5\gamma^3 - 2\beta^3 - 30\beta,$$
$$t_7 = 5\gamma^3 - \beta^3 - 45\beta. \tag{52}$$

References

1. Stokes GG (1851) Trans Camb Philos Soc 9:8–106
2. Napper DH (1983) Polymeric stabilization of colloidal dispersions. Academic, London
3. Anderson JL, Solomentsev Y (1996) Chem Eng Commun 148–150:291–314
4. Wunderlich RW (1982) J Colloid Interface Sci 88:385–397
5. Sasaki S (1985) Colloid Polym Sci 263:935–940
6. Ooms G, Mijnlieff PF, Beckers HL (1970) J Chem Phys 53:4123–4130
7. Matsumoto K, Suganuma A (1977) Chem Eng Sci 32:445–447
8. Anderson JL, Kim J (1987) J Chem Phys 86:5163–5172
9. Masliyah JH, Neale G, Malysa K, van de Ven TGM (1987) Chem Eng Sci 42:245–253
10. Veerapaneni S, Wiesner MR (1996) J Colloid Interface Sci 177:45–57
11. Solomentsev Y, Kotov A, Starov V (1992) Int J Multiphase Flow 18:739–750
12. Chen SB (1998) Phys Fluids 10:1550–1563
13. Kuo J, Keh HJ (1997) J Colloid Interface Sci 195:353–367
14. Batchelor GK (1972) J Fluid Mech 52:245–267
15. Reed CC, Anderson JL (1980) AIChE J 26:816–827
16. Happel J (1958) AIChE J 4:197–201
17. Kuwabara S (1959) J Phys Soc Jpn 14:527–533
18. Happel J, Brenner H (1983) Low Reynolds number hydrodynamics. Nijhoff, Dordrecht
19. Prasad D, Narayan K A, Chhabra RP (1990) Int J Eng Sci 28:215–230
20. Koplik J, Levine H, Zee A (1983) Phys Fluids 26:2864–2870
21. Neale G, Epstein N, Nader W (1973) Chem Eng Sci 28:1865–1874
22. Levine S, Neale GH (1974) J Colloid Interface Sci 47:520–529
23. Chen SB, Cai A (1999) J Colloid Interface Sci 217:328–340